nature nanotechnology

ARTICLES

https://doi.org/10.1038/s41565-021-00959-4

Unveiling the full reaction path of the Suzuki–Miyaura cross-coupling in a single-molecule junction

Chen Yang[1,8], Lei Zhang[2,8], Chenxi Lu[3,8], Shuyao Zhou[1], Xingxing Li[4], Yanwei Li[3,5], Yang Yang[6], Yu Li[1], Zhirong Liu[1], Jinlong Yang[4], K. N. Houk[3]✉, Fanyang Mo[2]✉ and Xuefeng Guo[1,7]✉

Conventional analytic techniques that measure ensemble averages and static disorder provide essential knowledge of the reaction mechanisms of organic and organometallic reactions. However, single-molecule junctions enable the in situ, label-free and non-destructive sensing of molecular reaction processes at the single-event level with an excellent temporal resolution. Here we deciphered the mechanism of Pd-catalysed Suzuki–Miyaura coupling by means of a high-resolution single-molecule platform. Through molecular engineering, we covalently integrated a single molecule Pd catalyst into nanogapped graphene point electrodes. We detected sequential electrical signals that originated from oxidative addition/ligand exchange, pretransmetallation, transmetallation and reductive elimination in a periodic pattern. Our analysis shows that the transmetallation is the rate-determining step of the catalytic cycle and clarifies the controversial transmetallation mechanism. Furthermore, we determined the kinetic and thermodynamic constants of each elementary step and the overall catalytic timescale of this Suzuki–Miyaura coupling. Our work establishes the single-molecule platform as a detection technology for catalytic organochemistry that can monitor transition-metal-catalysed reactions in real time.

As the central science of chemical synthesis, catalysis enjoys widespread applications, which range from the manufacturing of valuable pharmaceuticals and agrochemicals to large-scale petroleum processing. To guide the further development of catalytic processes, mechanistic investigations offer critical insights into fundamental chemical principles and catalyst's structure–activity relationships. However, such studies on complex catalytic organic and organometallic processes continue to face numerous challenges. Although conventional macroscopic technologies used in mechanistic investigation have assisted chemists to construct the basis of catalytic reaction mechanisms, novel technologies are needed to obtain more insight into catalytic reactions beyond displaying ensemble averages and static disorder[1]. Single-molecule detection, in particular single-molecule electrical detection, can visualize molecular behaviour and dynamic disorder at the single-molecule or single-event level with a high time resolution[2–5]. As with the dominant conductive channel in molecular nanocircuits, the single-molecular conductance monitored during the course of the reaction is faithfully synchronous to the molecular structure[6–8]. In addition, covalently bonded graphene-based single-molecule devices show a high device stability that can withstand chemical treatments and external stimuli, and thus display the capability of long-term, real-time monitoring. By analysing the dynamic behaviour and reaction trajectory of a single catalyst embedded in the single-molecule platform, an enormous amount of mechanistic information, which includes the kinetic and thermodynamic parameters of every single elementary step, can be conveniently extrapolated, and thereby afford a powerful tool to interrogate the mechanism of catalytic processes.

Suzuki–Miyaura cross-coupling has emerged as one of the most widely used methods for the construction of C–C bonds due to its demonstrated efficiency, broad functional group compatibility and the ready availability of air-stable, non-toxic organoboron reagents[9,10]. The flourishment of Suzuki–Miyaura cross-coupling is inseparable from extensive efforts and ingenious experiments dedicated to its mechanistic study by the chemistry community. However, the transmetallation step, namely, the migration of the organic moiety from boron to palladium, is still not well-understood. Recent breakthroughs revealed the existence of pretransmetallation intermediates that contained a Pd–O–B bond at low temperatures[11–13]. However, the lack of convenient time-resolved methods to detect the pretransmetallation and transmetallation intermediates at the molecular level hampers further study under catalytically relevant conditions. In addition, debates concerning two possible transmetallation mechanisms[14] have persisted for decades[15–17]. In the first mechanism, ligand exchange of an oxidative addition complex LPd(Ar)X (L, ligand; Ar, aromatic group; X, halide) with a base generates LPd(Ar)(OR), which then interacts with boronic acid to provide the transmetallation complex LPd(Ar)(Ar′). In the second mechanism, LPd(Ar)X directly undergoes transmetallation with the base-activated ate complex $Ar'B(OH)_2(OR)^-$ to produce LPd(Ar)(Ar′). Despite previous mechanistic studies on the

[1]Beijing National Laboratory for Molecular Sciences, State Key Laboratory for Structural Chemistry of Unstable and Stable Species, College of Chemistry and Molecular Engineering, Peking University, Beijing, P. R. China. [2]Department of Energy and Resources Engineering, College of Engineering, Peking University, Beijing, P. R. China. [3]Department of Chemistry and Biochemistry, University of California, Los Angeles, CA, USA. [4]Hefei National Laboratory for Physical Sciences at Microscale, University of Science and Technology of China, Hefei, P. R. China. [5]Environment Research Institute, Shandong University, Qingdao, P. R. China. [6]Department of Chemistry and Biochemistry, University of California, Santa Barbara, CA, USA. [7]Center of Single-Molecule Sciences, Institute of Modern Optics, College of Electronic Information and Optical Engineering, Nankai University, Tianjin, P. R. China. [8]These authors contributed equally: Chen Yang, Lei Zhang, Chenxi Lu. ✉e-mail: houk@chem.ucla.edu; fmo@pku.edu.cn; guoxf@pku.edu.cn

transmetallation mechanism using model systems[14,18], unambiguous differentiation of the two mechanisms with highly active Pd catalysts has been a non-trivial task. Single-molecule detection represents a potentially powerful technique to decipher the mechanism of transition-metal-catalysed reactions. Label-free, non-destructive single-molecule electrical monitoring directly measures the time trajectories and reaction pathways of individual intermediates[19,20] and transition states[21] in chemical processes, and thus furnishes exciting opportunities to better understand the mechanism of Suzuki–Miyaura cross-coupling. In this study, we report an electrical single-molecule platform that offers the full description of Suzuki–Miyaura cross-coupling facilitated by a widely used N-heterocyclic carbene (NHC)-supported Pd catalyst.

Device fabrication and characterization

Molecular engineering methods[22] (Fig. 1a) were used to build a single-molecule platform to monitor the Suzuki–Miyaura cross-coupling in real time. A single catalyst was integrated into a nanocircuit and its structural change during the catalytic process could be recorded by electrical signals. Pd(NHC)(cinnamyl)Cl, which has been investigated adequately in both experiments (including pre-activation) and theoretical calculations[23–27], was chosen as the functional centre of the molecular bridge. A molecular bridge (compound **3**) that contained an NHC–Pd with azido-functionalized side arms was synthesized in three steps from compound **1** (Fig. 1b). Graphene field-effect transistors were prepared by transferring graphene (grown by chemical vapour deposition) from copper sheets to silicon chips, followed by photolithography and metal-electrode evaporation. Compound **3** was then covalently integrated into nanogapped 2-hydroxydiphenylphosphinylbenzene-activated carboxyl terminal graphene point electrode pairs, which were fabricated through electron-beam lithography, oxygen plasma etching and chemical modification successively, to form stable graphene–molecule–graphene single-molecule junctions (GMG SMJs)[28] (Fig. 2a). More details of the molecular synthesis and device preparation are provided in Methods and Supplementary Sections 1–3 and Supplementary Figs. 1 and 2). Comparison of the current–voltage (*I*–*V*) curves before (no response) and after (response to some extent) integration showed the successful incorporation of the molecular bridges (Fig. 2b). With optimized conditions, the conjugation yield reached ~17% and ~16 of 92 devices on the same silicon chip showed a current response to voltage changes (Supplementary Fig. 3). The statistical analysis in the Supplementary Section 4 shows that the current response with a ~92% probability originates from an only-one-molecule connection between the electrodes. More importantly, this was confirmed using a combination of a super-resolution fluorescence microscope and high-speed sampling of the electrical monitoring system (Supplementary Fig. 4). Owing to non-radiative energy and/or charge transfer from the functional centre to the graphene electrodes[29], the successive cross-coupling of fluorescent 3-bromoperylene and *p*-methoxyphenylboronic acid catalysed by Pd on the GMG SMJ caused blinking at the single-molecule site. This resulted in a stochastic optical reconstruction microscopy effect, which provides a single-molecule-resolution fluorescence image between the electrodes[30]. This observation proved that only one catalyst molecule was connected between the pair of electrodes (Fig. 2c and Supplementary Fig. 5). In addition, the characteristic fluorescence spectrum of the product at the single-molecule site was detected, which proves that the catalyst worked (Supplementary Figs. 6–8). Furthermore, the change in the fluorescent intensity at this site was fully in accord with the GMG SMJ electrical signal, which displayed its dynamic behaviour (Fig. 2d and Supplementary Video 1), which again strongly proved the single-molecule conjunction and shows that the catalyst centre is, indeed, in the catalytic process.

Conductance-state analysis

Owing to its superior temporal resolution and high levels of molecular-conductance sensitivity towards chemical transformations, we focused on electrical signals for the study of this Suzuki–Miyaura coupling. A 300 mV bias voltage was applied at 298 K to the molecular bridge with the nanoamp-level current sampled at 57.6 kHz. A current signal level (~15 nA, conductance state 0) with no significant fluctuation (which mainly originated from the instrument noise, <500 pA) was observed (Fig. 3a). Statistical results with a Gaussian distribution indicated no GMG SMJ structure changes (Fig. 3b). After adding a dimethylformamide (DMF) solution of KO^{t}Bu to the home-made reaction cell, the current level dropped to ~11 nA (conductance state 1), which indicates a change in the GMG SMJ structure. Control experiments with an open circuit (Supplementary Fig. 9), a graphene homojunction (Supplementary Figs. 10 and 11), an imidazolium salt single-molecule heterojunction (Supplementary Fig. 12) and a single-molecule catalyst device with product biphenyl (Supplementary Fig. 13) at different temperatures (Supplementary Fig. 14) were conducted in the same reaction conditions. These showed that the current change indeed originated from the Pd centre and eliminated the potential interference of molecular circuit noises. Previous studies indicated that this change should correspond to the pre-activation process that forms a Pd(0) ready to enter the catalytic cycle[31,32]. Note that the process to form a Pd(I) dimer during the pre-activation process can be avoided in the single-molecule Suzuki–Miyaura cross-coupling reaction[33–35]. The inelastic electron tunnelling spectrum (IETS) of the Pd(0) device at 2 K (Supplementary Figs. 15a and 16a) supports this attribution. After achieving the Pd(0) device, we then focused the study of the following catalytic cycle. After thoroughly washing the reaction cell with DMF to remove residual KO^{t}Bu, the addition of a PhBr solution (the results from other kinds of halogenated benzenes are provided in Supplementary Figs. 17 and 18) significantly increased the current level to ~52 nA (conductance state 2), which shows that the oxidative addition occurred[10,31]. After the addition of KO^{t}Bu, the current then dropped to ~20 nA (conductance state 3), which implies a ligand exchange[36,37] (Fig. 3a), which was further supported by its IETS at 2 K (Supplementary Fig. 16). After the addition of $PhB(OH)_2$, sequential, periodic transitions of the current levels (Fig. 3c) among the four stable states (conductance states 1 and 3, and new states 4 and 5 (Fig. 3d), and the frequency statistics in Fig. 3e) correspond to the four intermediates (Fig. 3f) observed in the *I*–*t* curve. The reaction system showed the most stable state (state 4) at a low temperature (Supplementary Fig. 15) and it was further assigned to the pretransmetallation complex through its IETS (Supplementary Fig. 16). This behaviour is characteristic of a catalytic reaction that takes place in the GMG SMJ (Fig. 3c, enlarged in Fig. 3d). Furthermore, intermediate-controlled control experiments (Fig. 4 and Supplementary Fig. 19) supported the assignment of the states and showed the regulation of catalysis. Excess base increased the state 3 ratio, which implies more ligand exchange (Fig. 4a,b). The conductivity stabilized at state 4 and could not go forward after replacing the phenylboronic acid with alkylboronic acid, which was classified as a species before transmetallation (Fig. 4c,d). State 5 can be prepared through another pathway: saturated biphenyl suppressed the reductive elimination process and its ratio became higher (Fig. 4e,f). Therefore, from low- to high-conductance states, these four species were assigned to be Pd(0), oxidative addition/ligand exchange complex, pretransmetallation complex and transmetallation complex, respectively (Fig. 3f), consistent with the theoretical simulation of the transmission spectra and *I*–*V* curves (Supplementary Figs. 20–22).

Simulation of potential energy surfaces

We further studied these species involved in this Suzuki–Miyaura coupling in GMG SMJ via density functional theory calculations

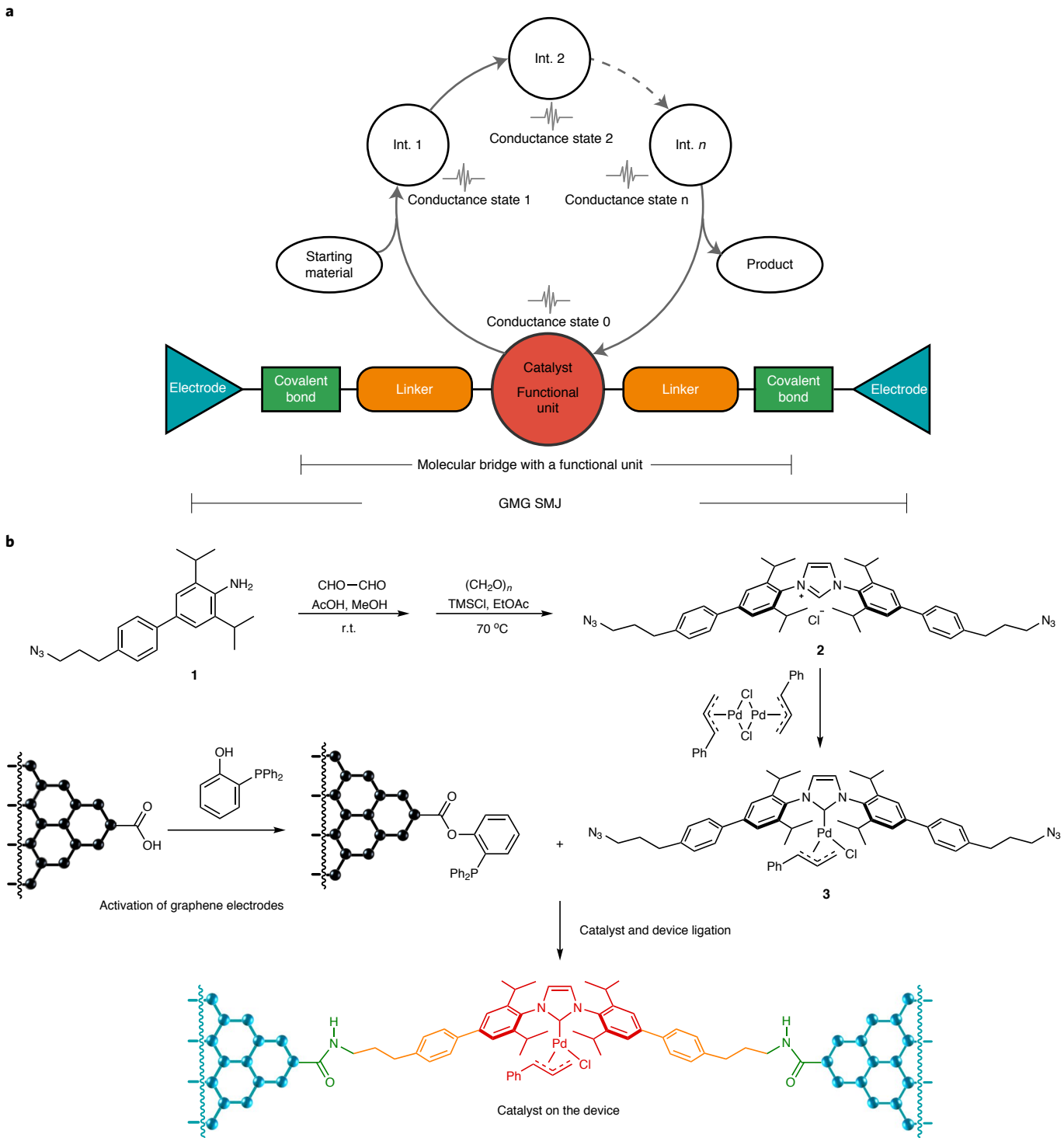

Fig. 1 | Design of a single-molecule catalyst device. a, Schematic strategy of the monitoring process for a single-molecule catalytic cycle. Real-time changes of the decoupled catalytic function centre would be detected in the current. **b**, Synthesis of molecular bridges, connection of individual Pd catalysts and anchoring of graphene point electrode pairs. Int, intermediate; r.t., room temperature; TMS, trimethylsilyl.

(the catalytic cycle is presented in Fig. 5 and the pre-activation process is presented in Supplementary Fig. 23). Two possible transmetallation pathways were computationally evaluated. In the first mechanism, LPd(Ar)X directly reacts with the base-activated ate complex $Ar'B(OH)_2(OR)^-$ (Fig. 5a). In the second mechanism, ligand exchange of the oxidative addition complex LPd(Ar)X with a base generates LPd(Ar)(OR) (conductance state 3) (Fig. 5b). These two paths converge on the previously characterized 'missing intermediate'[11]—a four-membered ring pretransmetallation complex (conductance state 4) (Fig. 6d). Calculations show that the ligand exchange reaction is highly exergonic, which indicates that a anion-exchange mechanism is probably operative. Based on this finding, according to the time-sequence relation, we assigned conductance state 1 to Pd(0) coordinated with PhX or Ph—Ph (INT1 or INT8), conductance state 3 to the oxidative addition/ligand exchange complex (INT3), conductance state 4 to the

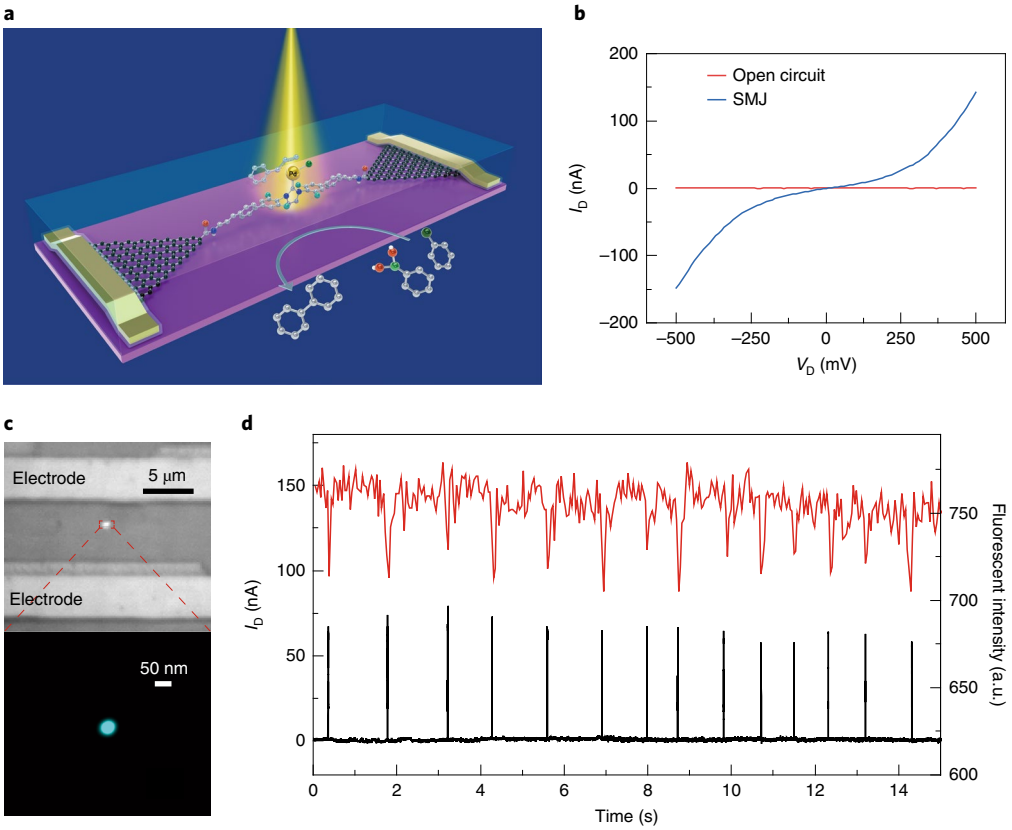

Fig. 2 | Preparation and characterization of a single-molecule catalyst device. a, Schematic of a single-molecule catalytic device for the simultaneous characterization of optical and electrical characteristics. **b**, *I*–*V* curves before and after preparation of the single-molecule device (D). The voltage response indicates the successful preparation of the single-molecule device. **c**, Fluorescent super-resolution imaging of the single-molecule catalyst during the reaction of 3-bromofluorene with phenylboronic acid. A 405 nm, 5 mW laser was focused on the graphene device through a ×100 oil lens with 5,000 photos taken with an exposure time of 50 ms. A single-molecule-resolution image was obtained after stochastic optical reconstruction. The fluorescent changes in the single-molecule functional centre were recorded. After removing the background, a bright spot was obtained with a diameter of about 50 nm, which indicates a single-molecule catalyst. The existence of only one ~50 nm spot between the metal electrodes (there are ~210 pairs of graphene electrodes with a distance of ~190 nm between each pair of metal electrodes) again indicated the successful preparation of the single-molecule device. **d**, After the excitation light and a 300 mV bias voltage were applied simultaneously at 298 K, the fluorescent signal of the single-molecule catalyst in real time was compared with the monitored current signal. a.u., arbitrary units.

pretransmetallation complex (INT4) and conductance state 5 to the transmetallation complex (INT7). All these assigned intermediates have relatively stable energy valleys in the potential energy surfaces.

Based on the time sequence of the conductance states, this single-molecule platform provides a simple and powerful method to distinguish between several possible reaction pathways. First, conductance state 2, which corresponds to the oxidative addition complex, was not observed in the catalysis cycles, which indicates an exceedingly short lifetime for the oxidative addition complex (<17 μs) and a rapid anion exchange with *tert*-butoxide. Further, in Fig. 3c,d, a large number of conductance states 3 and 4 appear in succession, which correspond to the transition from the oxidative addition/ligand exchange complex (INT3) to pretransmetallation complex (INT4) (Fig. 5b). Taken together, this analysis clarifies that anion-exchange precedes transmetallation. Thus, these findings demonstrate in the Suzuki–Miyaura cross-coupling catalysed by NHC-based Pd complexes that transmetallation also occurs via an anion-exchange-first mechanism[16,17].

Single-molecule thermodynamics and kinetics

In addition, the high solvent compatibility and determined interface coupling may allow our single-molecule devices to be very stable under complex conditions, which involve various temperatures, substrates and solvents. *I*–*t* curves recorded on more than one device (another set of data is provided in Supplementary Section 11) for five temperatures (258, 278, 298, 318 and 338 K) indicated accelerated conductance changes, which shows faster reactions at higher temperatures (Fig. 6a, enlarged in Fig. 6b). We also investigated the effect of *para*-substituents on the aromatic ring of the boronic acid on the reaction rate at 298 K (Supplementary Fig. 24 and Supplementary Table 1). In this Hammett study, an excellent linear relationship between $\log(k_x/k_H)$ and σ_p was obtained (Fig. 6c), where k_x and k_H are the rate constants of the reaction with *para*-substituted and non-substituted phenylboronic acids, respectively, and σ_p is the *para*-substituent constant. The positive ρ of +3.34 demonstrates that electron-withdrawing substituents accelerate the reaction, which indicates the importance of the association of LPd(Ar)(O^{t}Bu) and boronic acid[14,38]. Single-molecule dynamics is also affected by the choice of the solvent, and the polar solvent was found to accelerate the overall reaction (Supplementary Fig. 25). Our single-molecule measurements of rate constants with a range of solvent showed a profound solvent effect on the oxidative addition step[39], which is consistent with the presence of the concerted three-centre transition state (with a certain extent of charge separation according to computational studies)[40]. In contrast, the transmetallation displayed a relatively small solvent effect, which is consistent with previous findings[11] (Supplementary Fig. 26).

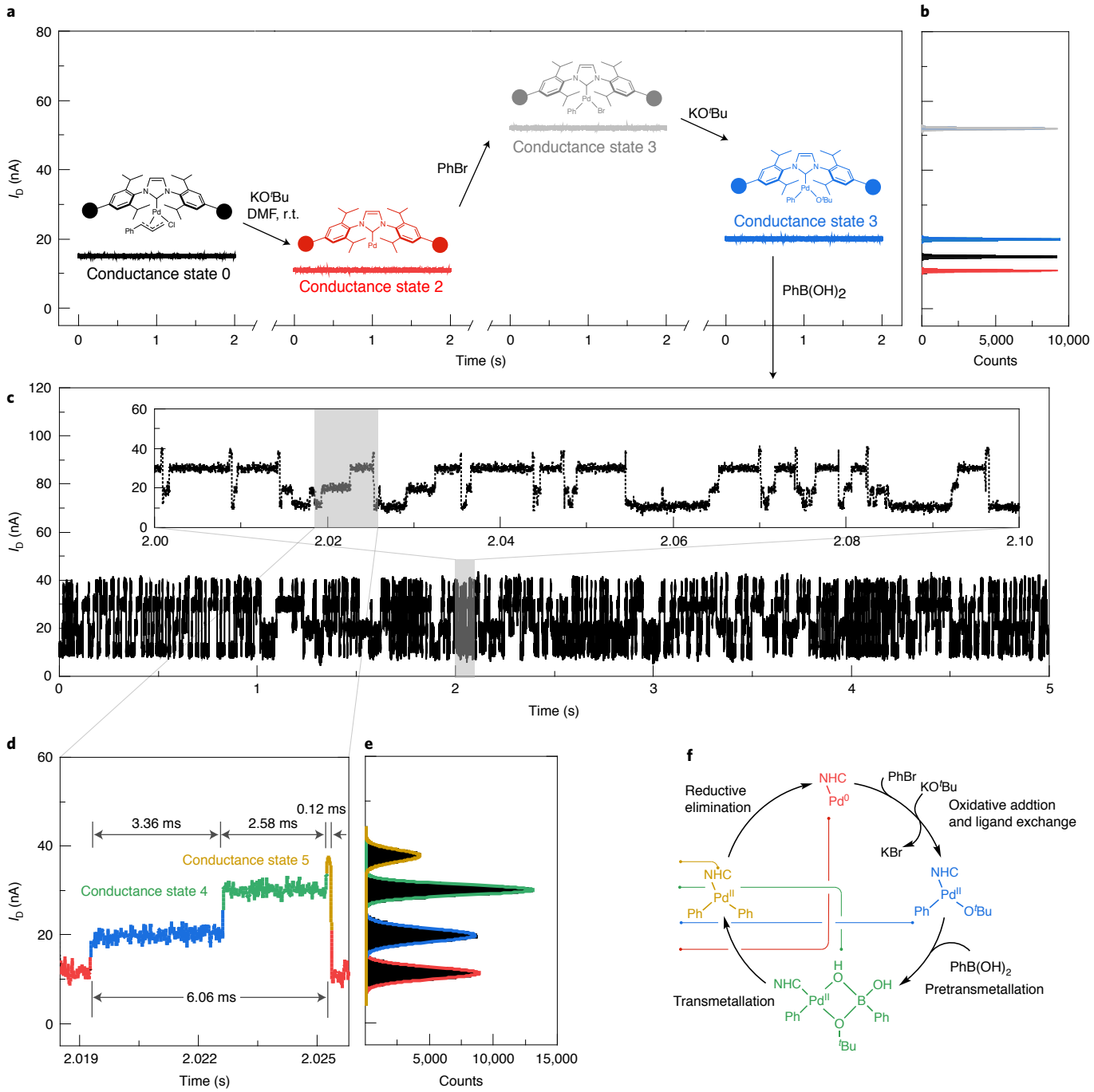

Fig. 3 | Electrical characterization and signal attribution of the single-molecule Suzuki–Miyaura cross-coupling reaction. a, Current signal variations with a bias voltage of 300 mV between the source and drain electrodes during the successive addition of the reaction substrates at 298 K. The catalyst underwent pre-activation, oxidative addition and ligand exchange through four conductance states. **b**, Analysis of the current frequency variations for these four conductance states. **c**, By adding phenylboronic acid to the substrates in **a**, the signal starts to switch between multiple states, shown for 5 s with an expanded trace that covers just 0.1 s. **d**, One catalytic cycle (extracted from **c**) showing four conductance states. **e**, Frequency distributions of all the current signals in **c**. **f**, Attributions of the four conductance states in the current signal. From low to high, they are Pd(0), the species after ligand exchange, the pretransmetallation species and the species before reductive elimination.

To extrapolate valuable kinetic constants of Suzuki–Miyaura coupling using a NHC-derived Pd catalyst, we focused on the coupling of PhBr and PhB(OH)$_2$ (both concentrations were 1 mM) at different temperatures (Fig. 6a). The hidden Markov model was applied to simulate the single-molecule behaviour for the monitored single-event process. After idealizing the *I*–*t* curve using QuB software (Supplementary Figs. 27 and 28), the state transfer rate (r) of the process was calculated (Fig. 6d,e, Supplementary Fig. 29 and Supplementary Table 2; more data are provided in Supplementary Figs. 30–33 and Supplementary Table 3) using the maximum interval likelihood rate estimate[41] according to $k = r = 1/\tau$ (approximated as a zero-order reaction at 1 mM according to the concentration-dependent measurements; Supplementary Figs. 34 and 35), where k is the rate constant and τ is the dwell time. The single

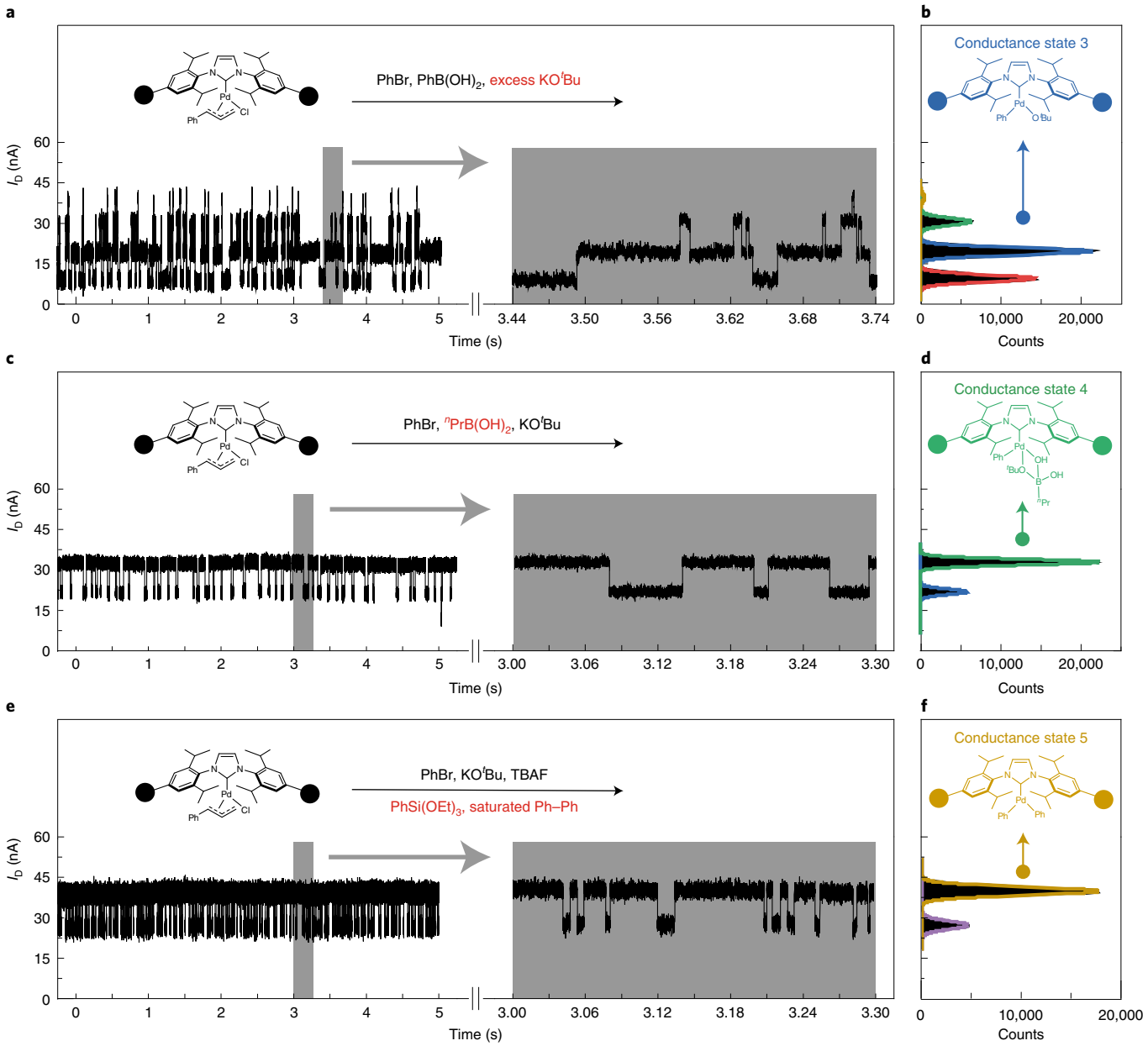

Fig. 4 | Intermediate-controlled experiments. a,**b**, *I*–*t* curves over 5 s with an enlargement (**a**) and the corresponding histogram (**b**) of the reaction after adding excess base. **c**,**d**, *I*–*t* curves over 5 s with an enlargement (**c**) and corresponding histogram (**d**) of the reaction with *n*-propylboronic acid. TBAF, tetrabutylammonium fluoride. **e**,**f**, *I*–*t* curves over 5 s with an enlargement (**e**) and the corresponding histogram (**f**) of the Hiyama reaction after adding saturated biphenyl.

elementary reaction rate constant was found to be higher than the ensemble measurements[13,42]. We reasoned that the following factors caused by the unique single-molecule electrical monitoring platform might have contributed to this observation: (1) more high-frequency reversible species conversions were recorded due to the high temporal resolution, (2) the maximum utilization of only one catalyst and (3) the presence of an external electrical field reduces the potential energy of each species (electrostatic catalysis effect; Supplementary Figs. 36–38)[43,44]. Based on single-molecule measurements, transmetallation was found to be the rate-limiting step in the catalytic cycle, which is consistent with our computational studies (overall barrier of ~65.3 kJ mol^{-1}; Fig. 5) and prior experimental findings[45]. Reductive elimination was found to be irreversible. Curve fits of the *I*–*t* curves showed that the average dwell time of conductance states 1 and 3–5 were 5.1 ± 0.4, 3.1 ± 0.1, 5.4 ± 0.1 and 1.4 ± 0.2 ms, respectively, with a time of 14.9 ± 0.7 ms for the average reaction period (Fig. 6f). The apparent turnover frequency (TOF) was $1/\Delta t = 67.0 \pm 3.0\,s^{-1}$, which does not account for any reversible processes. Counting catalytic cycles in the entire current signal gave a corrected TOF ($29.6 \pm 2.4\,s^{-1}$), which is higher than that reported in the literature[31], presumably due to the maximum utilization of only one catalyst.

Temperature gradient experimental data were plotted as ln *k* versus 1,000/T according to the Arrhenius equation to obtain the activation energies (E_a) of the forward and reverse reactions in the four elementary processes (Fig. 6g). The Eyring equation was then used to calculate $\Delta G^{\ddagger}$, $\Delta H^{\ddagger}$ and $\Delta S^{\ddagger}$ for the reaction (detailed information in Supplementary Tables 4 and 5). The thermodynamic data for the entire reaction were then $\Delta G = -13.8 \pm 1.1$ kJ mol^{-1},

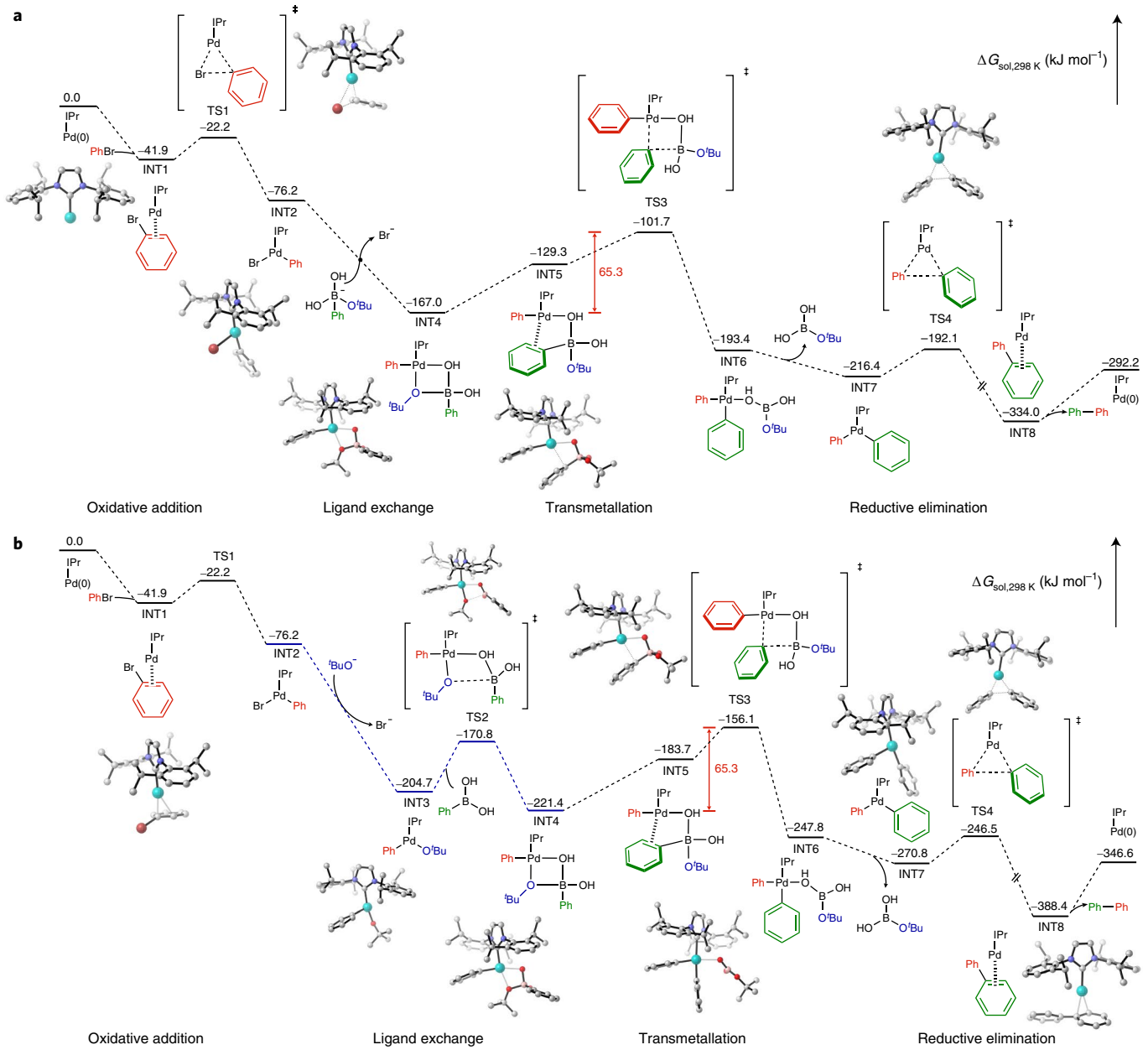

Fig. 5 | Theoretical potential energy surface calculation of the single-molecule Suzuki–Miyaura cross-coupling reaction. a, Potential energy surface of the oxidative addition species for transmetallation via trihydroxyborate. **b**, Potential energy surface of oxidative addition species for transmetallation via phenylboronic acid after ligand exchange. Gibbs free energies (kJ mol^{-1}) and intermediate structures are given in the figure. TS, transition state; IPr, bis(2,6-diisopropylphenyl)imidazo-2-ylidene.

$\Delta H = -54.6 \pm 1.3\,\mathrm{kJ\,mol^{-1}}$ and $\Delta S = -137.0 \pm 4.0\,\mathrm{J\,mol^{-1}\,K^{-1}}$. In addition, the maximum likelihood method was used to describe the mutual transformation between conductance state 1 and conductance state 4. The transfer rates of k_{14} and k_{41} were determined to be 5.9 ± 0.3 and $2.7 \pm 1.0 \times 10^{-4}\,\mathrm{s^{-1}}$, respectively, at 298 K (Supplementary Table 2). This indicates less interconversion between conductance state 1 and conductance state 4, even on the addition of water to promote the formation of boronate with different bases (Supplementary Fig. 39), which precludes the direct formation of a pretransmetallation four-membered ring complex without ligand exchange as a dominant path. This corroborates our findings on transmetallation as it favours a transmetallation mechanism that involves the anion-exchange complex LPd(Ar)(O^{t}Bu).

Conclusion

In summary, the faithful synchronization of the electrical signal and catalyst structure on an in situ, label-free and high-resolution single-molecule detection platform enabled us to elucidate the reaction trajectories and clarify the two long-term controversial pathways. The clarification of the catalytic reaction mechanism should help to further design high-performance catalysts and optimize reaction conditions, and so approach a higher efficiency and atom economy of the Suzuki–Miyaura cross-coupling. To achieve a more reliable detection technology, a high-throughput electrode fabrication method with atom-level precision needs to be developed to decrease the variation from device to device. This single-molecule platform

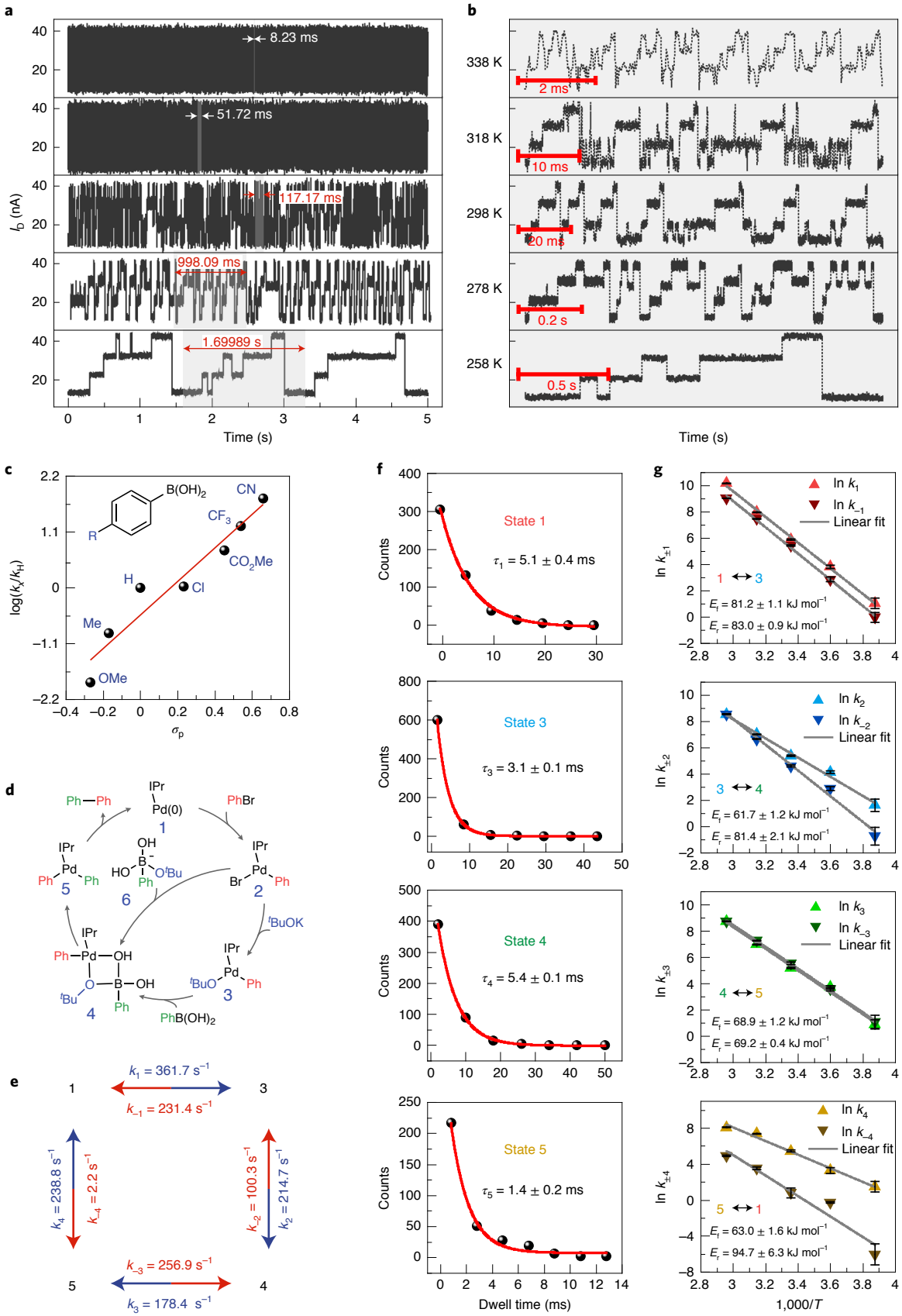

offers exciting opportunities to uncover active hidden intermediates and even probe the properties of transition states, and so afford a powerful tool to elucidate the mechanisms of various fundamental chemical and biological processes.

Online content

Any methods, additional references, Nature Research reporting summaries, source data, extended data, supplementary information, acknowledgements, peer review information; details of

Fig. 6 | Dynamic characterization of a single-molecule Suzuki–Miyaura cross-coupling reaction. a,**b**, *I*–*t* curves (5 s) of PhBr and $PhB(OH)_2$ in five temperature ranges from 258 to 338 K at 300 mV (**a**) and selected time windows with lengths of 1.69989 s, 998.09 ms, 117.17 ms, 51.72 ms and 8.23 ms (**b**). **c**, Substituent effect of the catalytic cycle. The fitting slope is 3.34 ± 0.34 and $R^2 = 0.93$. **d**, Possible catalytic cycle paths of the ensemble Suzuki–Miyaura cross-coupling reaction via states 1–6. **e**, Maximum likelihood method fitting results for the conversion rate between species 1, 3, 4 and 5 in the single-molecule experiments at 298 K. **f**, Time intervals of the four intermediates from idealized *I*–*t* curves at 298 K. Each intermediate lifetime was obtained by fitting a single exponential. **g**, Arrhenius plots of the forward and reverse reactions for states 1–5. The E_a values of the forward (E_f) and reverse (E_r) reactions were obtained by fits of the rate constants at the various temperatures using $\ln k = -\frac{E_a}{R \times 1{,}000} \times \frac{1{,}000}{T}$. The error scales (standard deviations) of ln *k* were obtained based on the statistics of ten measurements.

author contributions and competing interests; and statements of data and code availability are available at https://doi.org/10.1038/s41565-021-00959-4.

Received: 25 February 2021; Accepted: 13 July 2021;
Published online: 02 September 2021

References

1. Coontz, R. Not so simple. *Science* **305**, 957–957 (2004).
2. Barkai, E., Jung, Y. & Silbey, R. Theory of single-molecule spectroscopy: beyond the ensemble average. *Annu. Rev. Phys. Chem.* **55**, 457–507 (2004).
3. Lu, H. P., Xun, L. Y. & Xie, X. S. Single-molecule enzymatic dynamics. *Science* **282**, 1877–1882 (1998).
4. Armani, A. M., Kulkarni, R. P., Fraser, S. E., Flagan, R. C. & Vahala, K. J. Label-free, single-molecule detection with optical microcavities. *Science* **317**, 783–787 (2007).
5. Li, Y., Yang, C. & Guo, X. Single-molecule electrical detection: a promising route toward the fundamental limits of chemistry and life science. *Acc. Chem. Res.* **53**, 159–169 (2020).
6. Aviram, A. & Ratner, M. A. Molecular rectifiers. *Chem. Phys. Lett.* **29**, 277–283 (1974).
7. Venkataraman, L. et al. Electronics and chemistry: varying single-molecule junction conductance using chemical substituents. *Nano Lett.* **7**, 502–506 (2007).
8. Su, T. A., Li, H., Steigerwald, M. L., Venkataraman, L. & Nuckolls, C. Stereoelectronic switching in single-molecule junctions. *Nat. Chem.* **7**, 215–220 (2015).
9. Miyaura, N. & Suzuki, A. Palladium-catalyzed cross-coupling reactions of organoboron compounds. *Chem. Rev.* **95**, 2457–2483 (1995).
10. Beletskaya, I. P., Alonso, F. & Tyurin, V. The Suzuki–Miyaura reaction after the Nobel prize. *Coord. Chem. Rev.* **385**, 137–173 (2019).
11. Thomas, A. A. & Denmark, S. E. Pre-transmetalation intermediates in the Suzuki–Miyaura reaction revealed: the missing link. *Science* **352**, 329–332 (2016).
12. Thomas, A. A., Wang, H., Zahrt, A. F. & Denmark, S. E. Structural, kinetic, and computational characterization of the elusive arylpalladium(II)boronate complexes in the Suzuki–Miyaura reaction. *J. Am. Chem. Soc.* **139**, 3805–3821 (2017).
13. Thomas, A. A., Zahrt, A. F., Delaney, C. P. & Denmark, S. E. Elucidating the role of the boronic esters in the Suzuki–Miyaura reaction: structural, kinetic, and computational investigations. *J. Am. Chem. Soc.* **140**, 4401–4416 (2018).
14. Lennox, A. J. J. & Lloyd-Jones, G. C. Transmetalation in the Suzuki–Miyaura coupling: the fork in the trail. *Angew. Chem. Int. Ed.* **52**, 7362–7370 (2013).
15. Matos, K. & Soderquist, J. A. Alkylboranes in the Suzuki–Miyaura coupling: stereochemical and mechanistic studies. *J. Org. Chem.* **63**, 461–470 (1998).
16. Carrow, B. P. & Hartwig, J. F. Distinguishing between pathways for transmetalation in Suzuki–Miyaura reactions. *J. Am. Chem. Soc.* **133**, 2116–2119 (2011).
17. Amatore, C., Jutand, A. & Le Duc, G. Kinetic data for the transmetalation/reductive elimination in palladium-catalyzed Suzuki–Miyaura reactions: unexpected triple role of hydroxide ions used as base. *Chem. Eur. J.* **17**, 2492–2503 (2011).
18. Braga, A. A. C., Ujaque, G. & Maseras, F. A DFT study of the full catalytic cycle of the Suzuki–Miyaura cross-coupling on a model system. *Organometallics* **25**, 3647–3658 (2006).
19. Gu, C. et al. Label-free dynamic detection of single-molecule nucleophilic-substitution reactions. *Nano Lett.* **18**, 4156–4162 (2018).
20. Guan, J. X. et al. Direct single-molecule dynamic detection of chemical reactions. *Sci. Adv.* **4**, eaar2177 (2018).
21. Polanyi, J. C. & Zewail, A. H. Direct observation of the transition-state. *Acc. Chem. Res.* **28**, 119–132 (1995).
22. Xin, N. et al. Concepts in the design and engineering of single-molecule electronic devices. *Nat. Rev. Phys.* **1**, 211–230 (2019).
23. Li, G. et al. Mechanistic study of Suzuki–Miyaura cross-coupling reactions of amides mediated by [Pd(NHC)(allyl)Cl] precatalysts. *ChemCatChem* **10**, 3096–3106 (2018).
24. Meconi, G. M. et al. Mechanism of the Suzuki–Miyaura cross-coupling reaction mediated by [Pd(NHC)(allyl)Cl] precatalysts. *Organometallics* **36**, 2088–2095 (2017).
25. Melvin, P. R., Balcells, D., Hazari, N. & Nova, A. Understanding precatalyst activation in cross-coupling reactions: alcohol facilitated reduction from Pd(II) to Pd(0) in precatalysts of the type (η^3-allyl)Pd(L)(Cl) and (η^3-indenyl)Pd(L)(Cl). *ACS Catal.* **5**, 5596–5606 (2015).
26. Zhou, T. et al. $[Pd(NHC)(\mu\text{-}Cl)Cl]_2$: versatile and highly reactive complexes for cross-coupling reactions that avoid formation of inactive Pd(I) off-cycle products. *iScience* **23**, 101377 (2020).
27. Balcells, D. & Nova, A. Designing Pd and Ni catalysts for cross-coupling reactions by minimizing off-cycle species. *ACS Catal.* **8**, 3499–3515 (2018).
28. Cao, Y. et al. Building high-throughput molecular junctions using indented graphene point contacts. *Angew. Chem. Int. Ed.* **51**, 12228–12232 (2012).
29. Gaudreau, L. et al. Universal distance-scaling of nonradiative energy transfer to graphene. *Nano Lett.* **13**, 2030–2035 (2013).
30. Rust, M. J., Bates, M. & Zhuang, X. Sub-diffraction-limit imaging by stochastic optical reconstruction microscopy (STORM). *Nat. Methods* **3**, 793–795 (2006).
31. Marion, N. et al. Modified (NHC)Pd(allyl)Cl (NHC = N-heterocyclic carbene) complexes for room-temperature Suzuki–Miyaura and Buchwald–Hartwig reactions. *J. Am. Chem. Soc.* **128**, 4101–4111 (2006).
32. Fantasia, S. & Nolan, S. P. A general synthetic route to mixed NHC-phosphane palladium(0) complexes (NHC = N-heterocyclic carbene). *Chem. Eur. J.* **14**, 6987–6993 (2008).
33. Hruszkewycz, D. P., Balcells, D., Guard, L. M., Hazari, N. & Tilset, M. Insight into the efficiency of cinnamyl-supported precatalysts for the Suzuki–Miyaura reaction: observation of Pd(I) dimers with bridging allyl ligands during catalysis. *J. Am. Chem. Soc.* **136**, 7300–7316 (2014).
34. Hruszkewycz, D. P. et al. Effect of 2-substituents on allyl-supported precatalysts for the Suzuki–Miyaura reaction: relating catalytic efficiency to the stability of palladium(I) bridging allyl dimers. *Organometallics* **34**, 381–394 (2015).
35. Melvin, P. R. et al. Design of a versatile and improved precatalyst scaffold for palladium-catalyzed cross-coupling: $(\eta^3\text{-}1\text{-}^t\text{Bu-indenyl})_2(\mu\text{-}Cl)_2Pd_2$. *ACS Catal.* **5**, 3680–3688 (2015).
36. Comanescu, C. C. & Iluc, V. M. EH (E = N, O) bond activation by a nucleophilic palladium carbene. *Polyhedron* **143**, 176–183 (2018).
37. Grushin, V. V. & Alper, H. The existence and stability of mononuclear and binuclear organopalladium hydroxo complexes, [(R3P)2Pd(R′)(OH)]and [(R3P)2Pd2(R′)2(μ-OH)2]. *Organometallics* **15**, 5242–5245 (1996).
38. Moriya, T., Miyaura, N. & Suzuki, A. Synthesis of allenes by palladium-catalyzed cross-coupling reaction of organoboron compounds with propargylic carbonates: transmetalation of organoboron compounds with (alkoxo)palladium complexes under neutral conditions. *Synlett* **1994**, 149–151 (1994).
39. Sherwood, J., Clark, J. H., Fairlamb, I. J. S. & Slattery, J. M. Solvent effects in palladium catalysed cross-coupling reactions. *Green Chem.* **21**, 2164–2213 (2019).
40. Senn, H. M. & Ziegler, T. Oxidative addition of aryl halides to palladium(0) complexes: a density-functional study including solvation. *Organometallics* **23**, 2980–2988 (2004).
41. Milescu, L. S., Yildiz, A., Selvin, P. R. & Sachs, F. Maximum likelihood estimation of molecular motor kinetics from staircase dwell-time sequences. *Biophys. J.* **91**, 1156–1168 (2006).
42. Barrios-Landeros, F., Carrow, B. P. & Hartwig, J. F. Effect of ligand steric properties and halide identity on the mechanism for oxidative addition of haloarenes to trialkylphosphine Pd(0) complexes. *J. Am. Chem. Soc.* **131**, 8141–8154 (2009).

43. Ciampi, S., Darwish, N., Aitken, H. M., Diez-Perez, I. & Coote, M. L. Harnessing electrostatic catalysis in single molecule, electrochemical and chemical systems: a rapidly growing experimental tool box. *Chem. Soc. Rev.* **47**, 5146–5164 (2018).
44. Shaik, S., Danovich, D., Joy, J., Wang, Z. & Stuyver, T. Electric-field mediated chemistry: uncovering and exploiting the potential of (oriented) electric fields to exert chemical catalysis and reaction control. *J. Am. Chem. Soc.* **142**, 12551–12562 (2020).
45. Wolfe, J. P., Singer, R. A., Yang, B. H. & Buchwald, S. L. Highly active palladium catalysts for Suzuki coupling reactions. *J. Am. Chem. Soc.* **121**, 9550–9561 (1999).

Methods

Device fabrication and molecular connection. Similar to the previous method[46], a single layer of high-quality graphene was grown on a 25-μm-thick copper sheet by high-temperature chemical vapour deposition. The graphene was transferred to a 1.5 cm × 1.5 cm silicon wafer with a 300 nm SiO_2 layer through PMMA 950. After that, the graphene was protected by a mask and etched by oxygen plasma to obtain a 40-μm-wide graphene strip. Layers of Cr (8 nm) and Au (60 nm) were then thermally evaporated as metal electrode arrays using the template method, with 40 nm SiO_2 evaporated onto the metal electrodes to prevent leakage into the solution phase. The prepared graphene transistor was etched with a dashed-line lithography method using electron-beam lithography to produce a graphene electrode array with a carboxyl acid terminal using plasma etching and electrical burning.

We added 10^{-3} mol l^{-1} of 2-hydroxydiphenylphosphinylbenzene, a 1-ethyl-3-(3-dimethylaminopropyl) carbodiimide super-dried CH_2Cl_2 solution, a catalytic amount of 4-dimethylaminopyridine and *i*-Pr_2NEt to the newly cut graphene device. The reaction was performed for 1.5 days under anhydrous and anaerobic conditions. After that, the device was removed and washed with ultra-dried CH_2Cl_2 and ultra-dried tetrahydrofuran (THF). This activated the carboxyl group with triphenylphosphine. A THF/H_2O (10:1) solution with 10^{-4} mol l^{-1} of the catalyst was added to the device with the reaction under anaerobic conditions for 1 day. Then, the device was removed, rinsed with THF and dried with flowing N_2. This connected the molecular bridge between the graphene electrode pairs with amide bonds.

Electrical characterization. The *I*–*V* curve was measured by an Agilent 4155C semiconductor parameter system and a Karl Suss (PM5) manual probe station. The IETS at 2 K were measured by a Physical Property Measurement System (PPMS) and a UHFLI lock-in amplifier. The auxiliary output of the HF2LI lock-in amplifier gave a constant bias of 300 mV for the *I*–*t* curve. The current signal of the molecular loop was amplified by a DL1211 amplifier and then recorded by a high-speed acquisition card from NIDAQ at a rate of 57,600 samples per second. An INSTEC hot and cold chuck (HCC214S, INSTEC) temperature-control module with an accuracy of 0.001 °C was placed under the device to regulate the reaction temperature. The error scales (standard deviations) in the thermodynamics and kinetics analyses were obtained based on the statistics of ten different devices. To have a better comparability between single-molecule studies and ensemble experiments, the maximum and minimum values were removed to obtain the trimmed mean.

Optical characterization. The silicon wafer was changed to 1.8 cm × 3.5 cm to ensure the compatibility of the objective lens with the electrical probe system. The probe was connected to the source and drain electrodes of the device and placed on a motorized stage (Zdeck). A Nikon Ni-E microscope with a ×100 objective lens was positioned in close contact with a ~100-μm-thick homemade polydimethylsiloxane microchannel on the device through the lens oil. The single-molecule device was excited by a 405 nm laser with an EMCCD (Andor) used to receive the feedback emitted light and the fluorescence spectra. The stochastic optical reconstruction microscopy process control cable was connected to the trigger terminal of the UHFLI lock-in amplifier to provide synchronous triggering. The reconstruction and analysis of the pictures used the Advanced Research software.

Theoretical calculation. All the structures were optimized at the B3LYP/6-31G(d) -LANL2DZ level of theory. Frequency calculations were performed to verify that intermediates have no imaginary frequency, whereas the transition structures have only one imaginary frequency. Single-point energy calculations were carried out at M06L/6-311++G(2d,p)-SDD level of theory. The SMD solvation model of DMF was included in both the geometric optimization and single point energy calculations. The reported Gibbs free energies were calculated at 298 K and 1 M. All the calculations were performed with Gaussian 09 software.

Data availability

The datasets used in this work are available online from the Zenodo repository at https://doi.org/10.5281/zenodo.4903414. Source data are provided with this paper.

References

46. Yang, C. et al. Electric field-catalyzed single-molecule Diels–Alder reaction dynamics. *Sci. Adv.* **7**, eabf0689 (2021).

Acknowledgements

We acknowledge primary financial support from the National Key R&D Program of China (2017YFA0204901), the National Natural Science Foundation of China (21727806, 21933001 and 21772003) and the Tencent Foundation through the XPLORER PRIZE. The research at UCLA was supported by the US National Science Foundation (CHE 1764328). S.Z. and Z.L. appreciate the support from the High-Performance Computing Platform of the Center for Life Science at Peking University.

Author contributions

X.G., F.M. and K.N.H. conceived and designed the experiments. C.Y., L.Z. and Yu Li fabricated the devices and performed the device measurements. L.Z. carried out the molecular synthesis. C.L., S.Z., X.L., Yanwei Li, Z.L. and J.Y. built and analysed the theoretical model and performed the quantum transport calculations. X.G., F.M., K.N.H., Y.Y., C.Y. and L.Z. analysed the data and wrote the paper. All the authors discussed the results and commented on the manuscript.

Competing interests

The authors declare no competing interests.

Additional information

Supplementary information The online version contains supplementary material available at https://doi.org/10.1038/s41565-021-00959-4.

Correspondence and requests for materials should be addressed to K.N.H., F.M. or X.G.

Peer review information *Nature Nanotechnology* thanks Nadim Darwish, Albert Poater and the other, anonymous, reviewer(s) for their contribution to the peer review of this work.

Reprints and permissions information is available at www.nature.com/reprints.